Contrasting storm-time radiation belt events with and without dropouts – the importance of CME shocks

Stanislaus Nnadih[1,2,3]; Lauren Blum[1]; Zheng Xiang[4]; Weichao Tu[5]; Xingzhi Lyu[5]; Maria E. Usanova[1]; Craig J. Rodger[6]

[1]Laboratory for Atmospheric and Space Physics, University of Colorado, Boulder, USA
[2] African Regional Center for Space Science and Technology Education in English, Ife, Nigeria
[3] South African National Space Agency, Hermanus, South Africa
[4]Department of Space Physics, School of Electronic Information, Wuhan University, China
[5]Department of Physics and Astronomy, West Virginia University, Morgantown, WV, USA
[6]Department of Physics, University of Otago, Dunedin, New Zealand

Corresponding authors: Stanislaus Nnadih (stan.nnadih@lasp.colorado.edu) and Lauren Blum (lauren.blum@lasp.colorado.edu)

Key Points:

- The response of the outer radiation belt is compared during three intense (Dst_min < -100nT) CME-driven geomagnetic storms
- The first two storms occurred following the arrival of shocks and exhibit characteristic "dropouts" of MeV electrons during the main phase
- The third CME was not preceded by a shock, resulting in different solar wind and magnetospheric conditions and an unusual "non-dropout"

Abstract

This study compares 3 different geomagnetic storms (designated as storms 1, 2, and 3) observed by NASA's Van Allen Probes within the spacecraft's first 50 days in orbit. These storms were CME-driven with minimum DST around -138, -100, and -106 nT, respectively. Storms 1 and 2 occurred following the arrival of fast-forward shocks, which compressed the magnetopause inward to about 6.5 R_E and 7.5 R_E, respectively, as a result of the increase in solar wind dynamic pressure and density. The inward magnetopause motion helped contribute to a rapid depletion of MeV electrons across the entire outer belt. For the 3rd storm, however, there was little or no dropout of MeV electrons in the heart of the outer belt during the storm main phase. This third storm was generated by a CME without an associated shock, and the magnetopause actually moved outward at the start of the storm, suppressing loss of electrons through the outer boundary. The study reveals that under certain solar wind driving conditions radiation belt electron dropouts may not occur, even during large geomagnetic storms (Dst_min < -100 nT).

1 Introduction

Earth's magnetosphere has a region, known as the radiation belt, divided into the inner belt, between ~ 1.5 and 2.5 Earth radii (R_E), and the outer belt, which lies between ~ 3 and ~ 7 R_E in the equatorial plane. Within these regions, the energetic charged particles (e.g., electrons and protons) are trapped due to the dipolar-like topology of the geomagnetic field, which converges at high latitudes giving rise to relatively minimum magnetic field strength around the geomagnetic equator (Spjeldvik and Rothwell, 1985). The energy range of these trapped particles spans between hundreds of keV and tens of MeV (Mauk et al., 2013), and can pose serious threats to the satellites within the radiation belt regions (Baker, 2001; Baker and Kanekal 1994; Wrenn, G. L. 1995; Wrenn et al., 2002).

The electrons in the inner belt are relatively stable (Abel and Thorn, 1998; Rodger and Clilverd, 2002) compared to the outer belt, which is highly dynamic with flux intensities changing drastically by order of magnitudes on timescales from minutes to days (Friedel et al., 2002; Shprits et al., 2008a). The variations of these electron fluxes are most often observed during geomagnetic storms, including those driven by Coronal Mass Ejections (CMEs) (Reeves et al., 2003, Li et al., 2013).

CMEs result from eruptions of plasmas and magnetic fields occurring on the surface of the Sun, as a consequence of the energy release processes in the corona (Gopalswamy, 2004; Yashiro et al., 2004; Wang and Zhang, 2007; Byrne et al., 2010; Manoharan and Mujiber Rahman, 2011; Webb and Howard, 2012; Fu et al., 2021). They can be classified as fast (> 500 km/s) or slow (< 500 km/s) (Gopalswamy et al., 2000; Filippor, 2019) depending on their relative speed to average solar wind speed (MacQueen and Fisher, 1983; Sheeley et al., 1999; Pant et al., 2021). When faster than the surrounding solar wind, they drive either fast-forward or fast-reversed shocks, during which a simultaneous increase in the magnetic field magnitude and plasma parameters or a decrease in the magnetic field magnitude, solar wind density, and an increase in the solar wind speed, respectively, is observed (Kilpua et al., 2015). Similarly, they can also drive forward and reserved slow mode shocks, although rarely observed (Chao and Olbert 1970; Richter et al., 1985; Whang et al., 1998; Ho et al., 1998; Zuo et al., 2006), during which one observes an increase in the plasma density, temperature, and bulk speed, and a decrease in the magnetic field (Ho et al., 1998; Zuo et al., 2006). These fast or slow mode shocks often lead to an increase or decrease in the ram pressure at Earth's magnetopause (Srivastava and Venkatarishnan, 2002). However, slow-moving CMEs do not drive shocks (Lugaz et al., 2017).

Numerous studies have investigated the impact of CMEs on the dynamics of the outer radiation belt. Radiation belt dropouts are one of the most intense dramatic variations in Earth's magnetosphere (Baker et al., 1994; Xiang et al., 2018), which occur when electron fluxes drop by several orders of magnitude over a broad range of energies, spatial locations and within a few hours during the main phase of geomagnetic storms (Friedel et al. 2002; Shprits et al. 2008a; Turner et al., 2012a). During these periods, the electrons are either transported through the magnetopause into interplanetary space, through the process known as magnetopause shadowing (Lotoaniu et al., 2010; Turner et al., 2012a) or they precipitate into the atmosphere (e.g., Rodger et al., 2010; Bortnik et al., 2014; Thorne, et al., 2010).

While magnetopause shadowing occurs when the magnetopause compresses inwards as a result of an increase in the solar wind dynamic pressure and can be accompanied by enhanced outward radial diffusion driven by ultra-low frequency (ULF) waves, (e.g. Turner et al., 2012; Tu et al., 2019), wave-particle interactions that induce pitch angle scattering of electrons are the primary cause of precipitation during geomagnetic storms (Millan and Thorne 2006; Tu et al., 2010; Thorne, 2010; Ni et al., 2017; Jaynes and Usanova, 2019). However, studies have shown that a combination of magnetopause shadowing with outward radial diffusion as well as precipitation is often needed to explain radiation belt dropouts (e.g., Li et al., 1997; Morley et al., 2010; Tu et al., 2010; Turner et al 2012b; Bruno et al., 2022). For instance, Turner et al. (2012b) use data from multiple spacecrafts e.g., THEMIS, GEOS, and NOAA-POES to show that the sudden electron depletion observed at the main phase of the storm on 06 January 2011 resulted from outward transport rather than loss into the atmosphere. Morley et al. (2010a; 2010b) use energetic particle measurement from GPS constellation to show that electron loss between $4 < L^* < 6$ at energies above > 230 keV results from magnetopause shadowing and /or outward diffusion as well as precipitation to the atmosphere due to wave-particle interactions. EMIC waves have been suggested to be a major contributor to MeV electron precipitation loss during storm-time dynamics (e.g. Shprits et al., 2017, Xiang et al., 2018), while other studies have shown that pitch angle scattering by multiple wave modes simultaneously (e.g. EMIC and chorus waves) can help produce observed radiation belt losses, particularly at $L<5$ (e.g. Gao et al., 2015, Mourenas et al., 2016, Boynton et al., 2017, Drozdov et al., 2020).

Using data from CRRES, Akebono, GPS, and LANL-GEO, Shprits et al. (2012b) found that 78% of 25 electron flux dropouts analyzed were associated with a sudden increase in the solar wind dynamic pressure. Several other studies have shown associations between dropouts and an increase in the solar wind dynamic pressure as well (e.g., Ni et al., 2013; Ohtani et al., 2009). These increases in the dynamic pressure often occur following the passage of the stream interface regions during which the magnetopause standoff distance moves inward to around 8 R_E (Morley et al., 2010). Boynton et al. (2016) found that dropout magnitude at $L=6.6$ was primarily controlled by the square of the solar wind dynamic pressure, while a similar analysis of dropouts observed by GPS at $L=4.2$ was better associated the cube of the southward IMF B_z component (B_s^3) (Boynton et al. 2017). Xiang et al. (2018) found a similar dependence of dropouts on radial distance, with those at $L^*>4.5$ likely due primarily to magnetopause shadowing, while precipitation into the atmosphere likely contributed to those at lower L^*. These studies highlight the importance of considering radial distance (or L shell/L*) as well as electron energy during radiation belt dropouts.

Although several efforts have been made to better understand the variations of electrons in the radiation belt during geomagnetic storms, and in particular the processes resulting in the rapid dropout of electrons at the main phase (Friedel et al. 2002; Shprits et al. 2008a; Turner et al., 2012a; Tu et al., 2019; Rodger et al., 2019), there are no studies to date that describe the storm-time radiation belt little or non-dropouts to understand when and where geomagnetic storms do not result in complete dropouts. Recent studies (e.g., Murphy et al., 2018) have shown that radiation belts usually have these dropout signatures but upon closer inspection, not all the time, at all energies, or at all radial distances. The main objective of this paper is to explore a large geomagnetic storm (Dst min ~ -106 nT) that did not show a dropout of MeV electrons within the outer zone and to attempt to understand when or why the outer belt behaves in this manner.

2 Observations

2.1 Electron Flux Measurement.

Figure 1 shows the electron flux measurements observed by Van Allen Probes in 2012, during the geomagnetic storms within the spacecraft's first 50 days in orbit. The first four panels (a, b, c, and d) of the Figure show the electron flux measured by the ECT-REPT and ECT-MagEIS instruments of the Probes at 335.5 KeV, 458.2 KeV, 2.30 MeV, and 4.50 MeV, respectively, while the last panel (e) shows the intensity of the storms designated as storm 1, 2 and 3.

Geomagnetic storms further referred to as 1 and 2, which occurred on 30th September – 1st October 2012, and 8-9 October 2012, respectively, were accompanied by an enhancement of the solar wind dynamic pressure leading to significant outward radial transport and magnetopause loss (Turner et al., 2014; Tu et al., 2014). These two storms have also been simulated using the Lyon-Fedder-Mobary MHD code coupled to the Rice Convection Model, to show the contribution of the magnetopause and ULF wave activity to radiation belt losses (Hudson et al., 2014). However, no studies described the "unexpected" little or non-depletion of electron flux at the main phase of storm 3 (12 -13th October 2012), which is the aim of this investigation.

As shown in Figure 1, spacecraft flux measurements show a loss of 4.5 MeV electrons throughout the entire radial extent of the outer belt during the main phases of storms 1 and 2. However, there was little or no dropout of relativistic electrons at the main phase of storm 3. We recall that dropouts in the radiation belt result from both adiabatic and non-adiabatic processes. While adiabatic effects alone often cannot explain the magnitude of loss observed during dropouts (Kim and Chan 1997; Li et al., 1997), to minimize any ambiguity and reveal the real loss, we next investigated the Phase Space Density (PSD) profiles calculated from the electron flux data of the REPT and MagEIS instruments of Van Allen Probes.

2.2 Phase Space Density

PSD describes the kinematic state of the radiation belt electrons using three momentum coordinates i.e., μ, K, and L^* (Schulz and Lanzerotti, 1974), where μ and K represent the first and second adiabatic invariants, respectively, and L*, commonly referred to as Roederer L, relating to the third adiabatic invariant (Roederer, 1970). One of the benefits of using invariants PSD is that PSD distribution in L* does not change when only adiabatic changes are occurring in the system (Stapes et al., 2022). Figure 2 (a) shows the PSD at fixed K (0.115 $G^{1/2}$ R_E) and varying values of μ (1585, and 2290 MeV/G) that were calculated following methods outlined in Xiang et al. (2017), which used the semiempirical Tsyganenko magnetic field model TS04 (Tsyganenko and Sitnov, 2005). These μ values correspond to about 2.3 – 2.9 MeV energies at L* = 4.

For these μ and K values, the plots clearly show relativistic electron loss at the main phases of the first and second storms at a range of L* spanning the entire outer radiation belt (i.e., between ~ 3 and ~ 6 Re), while storm 3 resulted in little or no electron loss, particularly towards the inner edge of the outer belt.

To unambiguously identify dropouts and little or no dropouts at various radial distances, PSD data were binned in L* (0.1) and in time (4 hours). Dropouts were then identified when the PSD dropped by a factor of greater than 5 within 8-hour intervals. These criteria have been used successfully by previous studies (e.g., Duncan, 2000; Xiang et al., 2018) to identify dropout events and to ensure that the depletion of electrons PSD is prompt and significant. Figure 2 panel (b) to (f) shows the temporal variation of the PSD at fixed μ and K values, and at various L* (3 to 5). Following Xiang et al. (2018), dropout events are circled in red and appended with a number that indicates the magnitude of the dropouts at these radial distances (L*).

At μ values (1585 and 2290 MeV/G) corresponding to multi-MeV electrons in Figure 2 (left and right), we observed no depletion of electrons between L* (3.5 to 4.5) for storm 3 compared to storms 1 and 2, which did show dropouts at these L*.

2.3. Solar wind parameters

To better understand the drivers of the dynamics within the magnetosphere during these events, we recall that various studies (e.g., Paulikas and Blake 1979; Blake et al., 1997; Hudson et al., 2014) have shown clear relationships between activities in the radiation belt and solar wind parameters (for instance the duration of the Bz -southward components of the magnetic field, dynamic pressure, density, IMF and speed). Thus, Figure 3 shows the solar wind parameters obtained from the OmniWeb database (https://omniweb.gsfc.nasa.gov/ow_min.html) for the period between September 25th to October 25th, 2012. The solar wind OMNI data were measured by multiple spacecraft (ACE, WIND, and DSCOVR), time-shifted, and then propagated to the nose of the Earth's bow shock to represent the conditions at that location (King and Papitashvili, 2005). As such, they approximately show the solar wind conditions inputs into the inner magnetosphere impacting radiation belt dynamics.

CME-driven geomagnetic storms occur when the southward interplanetary magnetic field either in the flux rope or sheath of the CME coincides with the northward field of the magnetosphere leading to the transfer of energy from the solar wind to the magnetosphere, and the enhancement of the ring current (Gosling, 1993; Dryer, 1994; Gonzalez et al., 1994; Gopalswamy et al., 2010; Green and Baker, 2015). This enhancement is observed by the 1-hour (DST) or 1-minute SYM-

H geomagnetic indices (Wanliss and Showalter, 2006), during which the Bz (GSM) component of the Interplanetary Magnetic Field (IMF) turned and remain negative for the duration of the main phase of the storm. Bz GSM < 0 allows significant magnetic reconnection on the dayside of the magnetosphere, leading to a build-up of the ring current, resulting in a weakening of the geomagnetic field as quantified by the SYM-H index. The sudden northward turning of Bz (Bz > 0) often signals the start of the recovery phase of the storm when internal magnetospheric processes work to absorb the energy deposited during the Bz southward interval.

The three geomagnetic storms investigated here were all driven by CMEs. Storms 1 and 2 occurred following the arrival of fast-forward shocks, which increased the magnetic field magnitude and other plasma parameters (e.g., density and dynamic pressure). However, there was no shock associated with storm 3, as shown in the shock data repository (http://ipshocks.fi/database), because the speed of the corresponding CME (~490 km/s) was slower when compared with the speed of the solar wind (~ 560 km/s).

The position of the magnetopause can be estimated using the Shue et al. (1997) magnetopause model, the output of which is shown in Figure 3f (black line). For the onset of storms 1 and 2, the magnetopause standoff distance moved inward to about 6.5 R_E and 7.5 R_E, respectively, as a result of an abrupt increase in solar wind dynamic pressure (~ 9.6 nPa, ~6.4 nPa) and density (~32 n/cc, ~22 n/cc), while at the onset of storm 3, the location of the magnetopause actually moved outward to around 14 R_E due a decrease in pressure (~ 0.2 nPa) and density (~0.5 n/cc), and then reached an inward minimum distance (~8 R_E) at the recovery phase of the storm, when the solar wind dynamic pressure and density increased to about 6.4 nPa and 12.5 n/cc, respectively, as a result of the arrival of a fast reversed shock (See Figure 3). To approximate the position of the last closed drift shell LCDS (the highest L shell for stable electron trapping within the magnetosphere), Albert et al. (2018) have shown that the shifted magnetopause position MP*= MP-2 is close to LCDS during storm times (see blue line on panel 3f). Furthermore, Pinto et al. (2018) showed that strong electron loss by outward radial diffusion is often observed down to L_{min}=MP*(or LCDS)-1.5. L_{min} reaches a value of 3.6 and 4.2 during the main phase of storms 1 and 2, respectively, while it reaches only 5.3 during the main phase of storm 3, which is consistent with no dropout being observed within ~L*=5 during the third storm.

Consistent with the patterns and findings presented in this study, an increase in the solar wind dynamic pressure and IMF have been shown to play important roles in driving storm-time radiation belt dropouts (Ohtani et al., 2009, Boynton et al. 2016, 2017), and relatively low dynamic pressure results in fewer electron dropouts in the magnetosphere (Yuan and Zong 2013). In addition to dynamic pressure playing a large role, a statistical study of about 110 CME-driven storms, subdivided into those with and without dropouts, showed that three quartiles of non-dropout storms correspond to the Dst signature above ~ -80 nT compared to ~ -125 nT for storms with dropouts. While Morley et al., (2010) have shown that one can still get dropouts of electrons for small Dst signatures (Dst ~ - min > - 50), this case study reveals that under certain conditions there may not be dropouts even for large storms.

2.4. Magnetopause shadowing versus precipitation loss

As described in the Introduction, radiation belt loss is primarily the result of two distinct mechanisms, magnetopause shadowing and precipitation into Earth's atmosphere. MeV electron dropouts, particularly towards the inner edge of the outer radiation belt, are not necessarily driven by magnetopause shadowing and can also be caused by precipitation induced by wave-particle interactions. The absence of magnetopause loss is thus a necessary but not sufficient condition for geomagnetic storms to result in non-dropouts, as wave-driven precipitation can also contribute to these dynamics. Section 2.3 discussed the role of solar wind driving and losses to the magnetopause, but solar wind conditions may also result in different magnetospheric conditions (and thus different wave environments and precipitation conditions) during these three storms. For example, high amplitude EMIC waves as well as dusk-sector precipitation have been shown to be enhanced during periods of high B_s (Clausen et al. 2011, Jun et al. 2019).

In order to explore the contribution of precipitation loss during these three storms, we utilize measurements from the low altitude Polar-orbiting Operational Environmental Satellites (POES). Figure 4 shows trapped and precipitating electron fluxes as measured by POES Medium Energy Proton and Electron Detector (MEPED) in the Space Environment Monitor-2 (SEM-2) instruments (Evans and Greer, 2004) during the period of interest in 2012. Top row presents electron measurements from the 90deg telescope, which points roughly perpendicular to the local magnetic field, at three different energies, >100 keV, >300 keV, and >~700 keV (as measured by the >6.9 MeV proton channel, P6, which responds primarily to high energy electrons when not exposed to energetic protons such as those from solar energetic particle events or the inner radiation belt; see Yando et al. 2011 for details). The middle panels show the same measurements from the zenith-pointing 0deg telescope, primarily responding to locally precipitating particles. The 90deg telescope primarily measures trapped and drift loss cone electrons, and thus typically shows dynamics similar to that of the trapped outer radiation belt (e.g. Claudepierre and O'Brien, 2020). While, with its 30deg field of view, the 0deg telescope does not encompass the entire loss cone at high latitudes and thus can underestimate precipitation loss during some periods, it provides a good indication of precipitation during periods of strong diffusion when the loss cone is close to full (e.g. Rodger et al. 2010, 2013). The bottom row shows the ratio of the 0 and 90deg telescopes, $j_{precip}/j_{trapped}$, to provide a rough estimate of the fraction of trapped electrons near the loss cone that precipitate into the atmosphere. When this ratio approaches 1, fluxes are more isotropic, suggesting strong scattering into the loss cone. One should note however that this parameter also approaches 1 when fluxes in both telescopes are close to background levels (e.g. much of P6, see panel k). Lastly, the rightmost column of Figure 4 shows slices of these three values (90deg telescope, 0deg telescope, and 0/90deg ratio) taken at L=4, in the heart of the outer radiation belt, for the three energies, >100keV (green), >300keV (blue), and >~700keV (red).

As seen in Figure 4, ~MeV electron precipitation into the atmosphere during all three of these storms is generally low, below the detection threshold of the POES P6 channel, particularly during the main phase dropout periods under investigation in this study. Some MeV electron precipitation can be observed at L=4 during storm 3 (see panels h and l), but little to none was measured during the main phase of storms 1 and 2. If we look at the >300 keV electron channel, we find a similar pattern, where storm 3 actually has an equal amount or more precipitation occurring across the outer radiation belt during the storm main phase, as compared to the radiation belt dropout periods of storms 1 and 2. This suggests that, while precipitation losses likely contribute somewhat to the net main phase dynamics of these three storms, a reduced level of magnetopause losses are likely the driver of the lack of a dropout during storm 3 as compared to 1 and 2.

3. Summary and Conclusion

In this paper, we compared 3 different geomagnetic storms (designated as storms 1, 2, and 3) observed by Van Allen Probes within the first 50 days in orbit. While the ECT-REPT and MagEIS instruments of the probes show full depletion (at L = 3 – 6) of electrons at 4.5 MeV for storms 1 and 2, there was little or no depletion of MeV electrons at the main phase of storm 3.

These 3 storms are all CME-driven, with DST_min ~ -138, -100, and -106 nT, respectively. While storms 1 and 2 were accompanied by fast-forward IP shocks, there was no shock associated with storm 3. The solar wind dynamic pressure, which is proportional to the proton density and solar wind speed square, is an important quantity in estimating the strength of the impact of an IP shock on the magnetosphere and is seen as a good indicator or predictor of geomagnetic activity (Srivastava and Venkatarishnan 2002).

During this study period, the shocks produced by the CMEs led to an increase in the density, dynamic pressure, and IMF B_z for storms 1 and 2, compressing the magnetopause and contributing to electron loss across the entire outer belt. However, although the intensity of storm 3 was significant (about -106 nT), there was actually a decrease in the pressure and large outward motion of the magnetopause during the onset of this storm, compared to the previous two storms. Little or no electron loss was observed at L* ~3.5 to 4.5, partly because there was no shock associated with the corresponding CME, to increase the ram pressure, compress the magnetopause and facilitate electron loss through magnetopause shadowing.

This case study has shown that under the right solar wind conditions, particularly low solar wind dynamic pressure, even large geomagnetic storms may not result in MeV electron dropouts. It underlines the importance of shocks associated with CME compared to CMEs without shocks in driving rapid radiation belt losses. Future work will expand this study to investigate statistically how typical, or rare, non-dropouts are in association with large geomagnetic storms, particularly in response to CMEs without shocks.

Acknowledgments

The authors wish to acknowledge the financial assistance from NASA Living With a Star program through Grant numbers 80NSSC21K1314 and 80NSSC21K1312, and also thank Harlan Spence and the ECT team for the Van Allen Probes MagEIS and REPT electron flux data (https://rbsp-ect.newmexicoconsortium.org/science/DataDirectories.php). The study equally uses data from the Heliospheric Shock Database (http://ipshocks.fi/database), generated and maintained at the University of Helsinki. The OMNI data was obtained from https://omniweb.gsfc.nasa.gov/ow_min.html. The authors are thankful to these teams for making their data available to the public. POES data are available here: https://www.ngdc.noaa.gov/stp/satellite/poes/dataaccess.html.

Figure Captions:

Figure 1. *Overview of the electron flux in the outer radiation belt observed by Van Allen Probes between September 25th to October 25th, 2012.*

Figure 2. *The electron PSD at μ = 1585 MeV/G, K = 0.115 $G^{1/2}$ R_E (left), and μ = 2290 MeV/G, K = 0.115 $G^{1/2}$ R_E (right), respectively for the geomagnetic storm between September 25th to October 25th, 2012. Panels (b) to (f) show the slices through the electron PSD at various L* values. The red circles denote dropout events, as defined by Xiang et al. (2018) study, with the number showing the magnitude of the dropouts.*

Figure 3. *Solar wind parameters for the geomagnetic storms were observed between September 25th to October 25th, 2012. (a) and (b) are the Bz and IMF in GSM coordinate, (c) total solar wind speed, (d) density, (e) solar wind dynamic pressure, (f) modeled subsolar magnetopause position (black) as well as the shifted magnetopause position, MP-2 (blue), (g) AE index showing substorm activities and (h) SYM-H index. The black vertical lines show the arrival of the IP shock as measured by the WIND spacecraft, while the onset and end of the main phases of the storms are denoted by the vertical red and blue dashed lines, respectively.*

Figure 4. *POES particle measurements at low Earth orbit from September 25th to October 25th, 2012. Top row shows particles measured in the 90 deg telescope, corresponding primarily to trapped and drift loss cone electrons, while the middle panel shows particles measured by the 0 deg telescope in the bounce loss cone. Bottom row shows the ratio of 0 to 90deg telescopes, or $j_{precip}/j_{trapped}$. Right-most column shows slices of these values taken at L=4. Timing of storms 1, 2, and 3 are labeled on the bottom left panel.*

References

Abel B. and R., Throne 1998 Electron scattering loss in Earth's inner magnetosphere 2. Sensitivity to model parameters Journal of Geophysical Research, VOL. 103, NO. A2, PAGES 2397-2407. https://agupubs.onlinelibrary.wiley.com/doi/abs/10.1029/97JA02920.

Albert, J. M., Selesnick, R., Morley, S. K., Henderson, M. G., & Kellerman, A. (2018). Calculation of last closed drift shells for the 2013 gem radiation belt challenge events. Journal of Geophysical Research: Space Physics, 123(11), 9597 9611. https://doi.org/10.1029/2018JA025991

Baker, D.N., et al. (1994). Relativistic electron acceleration and decay time scale in the inner and outer radiation belts: SAMPEX, *Geophys. Res. Lett.*, *21*(6), 409–412, doi:10.1029/93GL03532.

Baker, D. N. (2001). Satellite anomalies due to space storms. In *Space storms and space weather hazards* (pp. 285–311). Dordrecht: Springer. https://doi.org/10.1007/978-94-010-0983-6_11

Baker, D. N., & Kanekal, S. G. (2008). Solar cycle changes, geomagnetic variations, and energetic particle properties in the inner magnetosphere. *Journal of Atmospheric and Solar-Terrestrial Physics*, *120*(9), 7357–7373. https://doi.org/10.1002/2015JA021466

Boynton, R. J., Mourenas, D., and Balikhin, M. A. (2016). Electron flux dropouts at geostationary earth orbit: Occurrences, magnitudes, and main driving factors. Journal of Geophysical Research: Space Physics, 121, 8448--8461. https://doi.org/10.1002/2016JA022916

Boynton, R. J., Mourenas, D., and Balikhin, M. A. (2017). Electron flux dropouts at L = 4.2 from Global Positioning System satellites: Occurrences, magnitudes, and main driving factors. Journal of Geophysical Research: Space Physics, 122, 11,428--11,441. https://doi.org/10.1002/2017JA024523

Bruno, A., Blum, L. W., de Nolfo, G. A., Kataoka, R., Torii, S., Greeley, A. D., et al. (2022). EMIC-wave-driven electron precipitation observed by CALET on the International Space Station. *Geophysical Research Letters*, *49*, e2021GL097529. https://doi.org/10.1029/2021GL097529

Byrne, J.P., et al. (2010). Propagation of an Earth-directed coronal mass ejection in three dimensions. *Nat. Commun.* 1:74 doi: 10.1038 / ncomms1077

Chao, J. K., and S. Olbert (1970), Observation of slow shocks in interplanetary space, J. Geophys. Res.,75, 6394.

Claudepierre S. G., & O'Brien, T. P. (2020). Specifying high-altitude electrons using low-altitude LEO systems: The SHELLS model. Space Weather, 18, e2019SW002402. https://doi.org/10.1029/2019SW002402

Clausen, L. B. N., J. B. H. Baker, J. M. Ruohoniemi, and H. J. Singer (2011), EMIC waves observed at geosynchronous orbit during solar minimum: Statistics and excitation, J. Geophys. Res.,116, A10205, doi:10.1029/2011JA016823.

Dryer, M. (1994), Interplanetary studies: Propagation of disturbance between the Sun and the Magnetosphere. Space Sci. reviews. 67, 363

Drozdov, A. Y., Usanova, M. E., Hudson, M. K., Allison, H. J., and Shprits,Y. Y. (2020). The role of hiss, chorus, and EMIC waves in the modeling of the dynamics of the multi-MeV radiation belt electrons. Journal of Geophysical Research: Space Physics,125, e2020JA028282. https://doi.org/10.1029/2020JA028282

Duncan, J. M. (2000). Factors of safety and reliability in geotechnical engineering. *Journal of Geotechnical and Geoenvironmental Engineering*, *126*(4), 307–316. https://doi.org/10.1061/(ASCE)1090-0241(2000)126:4(307)

Evans, D. S., and M. S. Greer (2004), Polar Orbiting Environmental Satellite Space Environment Monitor–2 Instrument Descriptions and Archive Data Documentation, NOAA Tech. Mem. 1.4, Space Environ. Lab., Boulder, Colorado.

Filippov, B 2019. Difference of source regions between fast and slow coronal mass ejections. Publication of the Astronomical Society of Australia, 36, E022. Doi:10.1017/pasa.2019.13

Friedel, R. H. W., G. D. Reeves, and T. Obara (2002), Relativistic electron dynamics in the inner magnetosphere – A review, J. Atmos. Sol. Terr. Phys., 64, 265–282

Fu, H.; Zheng, Y.; Ye, Y.; Feng, X.; Liu, C.; Ma, H. (2021), Joint Geoeffectiveness and Arrival Time Prediction of CMEs by a Unified Deep Learning Framework. Remote Sens. 13, 1738. https://doi.org/ 10.3390/rs13091738

Gao, X., W. Li, J. Bortnik, R. M. Thorne, Q. Lu, Q. Ma, X. Tao, and S. Wang (2015), The effect of different solar wind parameters upon significant relativistic electron flux dropouts in the magnetosphere, J. Geophys. Res. Space Physics,120, 4324-4337, doi:10.1002/2015JA021182

Gonzalez, W. D., Joselyn, J. A., Kamide, Y., Kroehl, H. W., Rostoker, G., Tsurutani, B. T. and Vasyliunas, V. M. (1994), What is a Geomagnetic Storm?, *J. Geophys. Res.* 99, 5771.

Gopalswamy, N. (2004). “A Global Picture of CMEs in the Inner Heliosphere,” in The Sun and the Heliosphere as an Integrated System. Editors G. Poletto and S. T. Suess (Dordrecht, The Netherlands: Astrophysics and Space Science Library), vol. 317, 201. doi:10.1007/978-1-4020-2666-9_8

Gopalswamy, N., Lara, A., Lepping, R. P., Kaiser, M. L., Berdichevsky, D., and Cyr,St. O. C. (2000). Interplanetary Acceleration of Coronal Mass Ejections. Geophys. Res. Lett. 27, 145–148. doi:10.1029/1999GL003639.

Gosling, J. T. (1993), The solar flare myth. Journal of Geophysical Research JGR, 98, 18937

Green, L., & Baker, D. (2015), Corona Mass Ejections; a driver of severe space weather. Wthr, 70, 31. https://doi.org/10.1002/wea.2437

Horne, R. B. et al. (2005). Wave acceleration of electrons in the Van Allen radiation belts. Nature 437, 227–230.

Ho, C. M., et al. (1998), A pair of forward and reverse slow-mode shocks detected by Ulysses at 5 AU, Geophys. Res. Lett.,25, 2613

Hudson, M. K., D. N. Baker, J. Goldstein, B. T. Kress, J. Paral, F. R. Toffoletto, and M. Wiltberger (2014), Simulated magnetopause losses and Van Allen Probe flux dropouts, Geophys. Res. Lett., 41,1113–1118, doi:10.1002/2014GL059222.

Jaynes, A. N., & Usanova, M. E. (Eds.) (2019). *The dynamic loss of Earth’s radiation belts from loss in the magnetosphere to particle precipitation in the atmosphere*. Amsterdam, Netherlands: Elsevier.

Jun, C.-W., Yue, C., Bortnik, J.,Lyons, L. R., Nishimura, Y. T.,Kletzing, C. A., et al. (2019). A statistical study of EMIC waves associated with and without energetic particle injection from the magnetotail. Journal of Geophysical Research: Space Physics,124, 433--450. https://doi.org/10.1029/2018JA02588

Kilpua, E. K. J., E. Lumme, K. Andreeova, A. Isavnin, and H. E. J. Koskinen (2015), Properties and drivers of fast interplanetary shocks near the orbit of the Earth (1995–2013), *J. Geophys.Res. Space Physics*, *120*, 4112–4125,doi:10.1002/2015JA021138

Kim, H.-J., and A. A. Chan (1997), Fully adiabatic changes in storm time relativistic electron fluxes, J. Geophys. Res., 102(A10), 22,107–22,116.

King, J. H., and N. E. Papitashvili (2005), Solar wind spatial scales in and comparisons of hourly Wind and ACE plasma and magnetic field data, J. Geophys. Res., 110, A02104, doi:10.1029/2004JA010649.

Lugaz Noé, Charles J. Farrugia, Reka M. Winslow, Colin R. Small, Thomas Manion, and Neel P. Savani (2017) Importance of CME Radial Expansion on the Ability of Slow CMEs to Drive Shocks. The Astrophysical Journal, 848:75 (11pp), 2017 October 20. https://doi.org/10.3847/1538-4357/aa8ef9

Li, X., D. N. Baker, M. Temerin, T. E. Cayton, E. G. D. Reeves, R. A. Christensen, J. B. Blake, M. D. Looper, R. Nakamura, and S. G. Kanekal (1997), Multi-satellite observations of the outer zone electron variation during the November 3–4, 1993 magnetic storm, J. Geophys. Res., 102(A7),14,123–14,140

Li, X., et al. (2013), First results from CSSWE CubeSat: Characteristics of relativistic electrons in the near-earth environment during the October 2012 magnetic storms, J. Geophys. Res. Space Physics, 118, 6489–6499, doi:10.1002/2013JA019342.

Loto'aniu, T. M., Singer, H. J., Waters, C. L., Angelopoulos, V., Mann, I. R., Elkington, S. R., & Bonnell, J. W. (2010). Relativistic electron loss due to ultralow frequency waves and enhanced outward radial diffusion. Journal of Geophysical Research, 115, A12245. https://doi.org/10.1029/2010JA015755.

MacQueen, R. M., and Fisher, R. R. (1983). The Kinematics of Solar Inner Coronal Transients. Solar Phys. 89, 89–102. doi:10.1007/BF00211955

Mauk, B. H., Fox, N. J., Kanekal, S. G., Kessel, R. L., Sibeck, D. G., & Ukhorskiy, A. (2013). Science objectives and rationale for the radiation belt storm probes mission. *Space Science Reviews*, *179*(1–4), 3–27. https://doi.org/10.1007/s11214-012-9908-y

Manoharan, P.K., Mujiber Rahman, A. (2011), Coronal mass ejections – propagation time and associated internal energy. *J. Atmos. Solar-Terr. Phys.* 73, 671.

Millan, R. M., and R. M. Thorne (2007), Review of radiation belt relativistic electron losses, J. Atmos. Sol. Terr. Phys., 69, 362 – 377.

Morley, S. K., Friedel, R. H. W., Cayton, T. E., & Noveroske, E. (2010a). A rapid, global and prolonged electron radiation belt dropout observed with the Global Positioning System constellation. Geophysical Research Letters, 37, L06102. https://doi.org/10.1029/2010GL042772

Morley K., Reinerh. W. Friedel, Emma. Spanswick, Geoffrey. Reeves, John. Steinberg, Josef koller, Thomas Cayton, and Evan Noveroske. 2010b. Proc. R. Soc. A (2010)466, 3329–3350 doi:10.1098/rspa.2010.0078

Mourenas, D., Artemyev, A. V., Ma, Q., Agapitov, O. V., and Li, W. (2016). Fast dropouts of multi-MeV electrons due to combined effects of EMIC and whistler mode waves. Geophysical Research Letters, 43, 4155--4163. https://doi.org/10.1002/2016GL068921

Murphy, K. R., Watt, C. E. J., Mann, I. R., Jonathan Rae, I., Sibeck, D. G., Boyd, A. J., et al. (2018). The global statistical response of the outer radiation belt during geomagnetic storms. *Geophysical Research Letters*, *45*, 3783–3792. https://doi.org/10.1002/2017GL076674

Ni, B., Y. Y. Shprits, R. H. W. Friedel, R. M. Thorne, M. Daae, and Y. Chen (2013), Responses of Earth’s radiation belts to solar wind dynamic pressure variations in 2002 analyzed using multi-satellite data and Kalman filtering, J. Geophys. Res. Space Physics, 118, doi:10.1002/jgra.50437

Ni, B., Bortnik, J., Nishimura, Y., Thorne, R. M., Li, W., Angelopoulos, V., et al. (2014). Chorus wave scattering responsible for the Earth’s dayside diffuse auroral precipitation: A detailed case study. *Journal of Geophysical Research: Space Physics*, *119*, 897–908. https://doi.org/10.1002/2013JA019507

Ni, B., Hua, M., Zhou, R., Yi, J., & Fu, S. (2017). Competition between outer zone electron scattering by plasmaspheric hiss and magnetosonic waves. *Geophysical Research Letters*, *44*, 3465–3474. https://doi.org/10.1002/2017GL072989

Pant, V., Majumdar, S., Patel, R., Chauhan, A., Banerjee, D. and Gopalswamy, N. (2021) Investigating Width Distribution of Slow and Fast CMEs in Solar Cycles 23 and 24. Front. Astron. Space Sci. 8:634358. doi: 10.3389/fspas.2021.634358

Paulikas, G. A., & Blake, J. B. (1979). Effects of the solar wind on magnetospheric dynamics: Energetic electrons at the synchronous orbit. *Quantitative Modeling of Magnetospheric Processes, Geophys. Monogr. Ser*, *21*, 180-202.

Pinto, V. A., Zhang, X.-J., Mourenas, D., Bortnik, J., Artemyev, A. V., Lyons, L. R., & Moya, P. S. (2020). On the confinement of ultrarelativistic electron remnant belts to low L shells. Journal of Geophysical Research: Space Physics, 125(3), e27469. https://doi.org/10.1029/2019JA027469

Ohtani, S., Y. Miyoshi, H. J. Singer, and J. M. Weygand (2009), On the loss of relativistic electrons at geosynchronous altitude: Its dependence on magnetic configurations and external conditions, J. Geophys. Res., 114, A01202, doi:10.1029/2008JA013391.

Reeves, G. D., K. L. McAdams, and R. H. W. Friedel, T. P. O'Brien (2003), Acceleration and loss of relativistic electrons during geomagnetic storms, Geophys. Res. Lett., 30(10), 1529, doi:10.1029/2002GL016513.

Reeves, G. D., et al. (2013). Electron acceleration in the heart of the Van Allen radiation belts. Science 341, 991–994.

Richter, A. K., Rosenbauer, H., Neubauer, F. M., and Ptitsyna, N. G. (1985), Solar wind observations associated with a slow forward shock wave at 0.31 AU, *J. Geophys. Res.*, 90(A8), 7581– 7586, doi:10.1029/JA090iA08p07581.

Rodger, C J, M A Clilverd, J Green, and M-M Lam (2010). Use of POES SEM-2 observations to examine radiation belt dynamics and energetic electron precipitation into the atmosphere, J. Geophys. Res., 115, A04202, doi:10.1029/2008JA014023.

Rodger, C. J., A. J. Kavanagh, M. A. Clilverd, and S. R. Marple (2013), Comparison between POES energetic electron precipitation observations and riometer absorptions: Implications for determining true precipitation fluxes, J. Geophys. Res. Space Physics, 118, doi:10.1002/2013JA019439.

Rodger, C. J., Turner, D. L., Clilverd, M. A., & Hendry, A. T. (2019). Magnetic local time-resolved examination of radiation belt dynamics during high-speed solar wind speed-triggered substorm clusters. Geophysical Research Letters,46 https://doi.org/10.1029/2019GL083712

Rodger, C. J., and M. A. Clilverd, (2002). Inner radiation belt electron lifetimes due to whistler-induced electron precipitation (WEP) driven losses, Geophys. Res. Lett.,29(19), 1924, doi:10.1029/2002GL015795.

Roederer, J. G. (1970), Dynamics of Geomagnetically Trapped Radiation, Springer, New York.

Roederer, J. G., & Lejosne, S. (2018). Coordinates for representing radiation belt particle flux. Journal of Geophysical Research: Space Physics, 123, 1381–1387. https://doi.org/10.1002/2017JA025053.

Spjeldvik, W. N., and P. L. Rothman (1985), The radiation belts, in Handbook of Geophysics and the Space Environment, edited by A. S. Jursa, chap. 3, p. 1, Air Force Geophys. Lab., Bedford, Mass.

Shprits, Y. Y., S. R. Elkington, N. P. Meredith, and D. Subbotin (2008a), Review of modeling losses and sources of relativistic electrons in the outer radiation belt I: Radial transport, J. Atmos. Sol. Terr. Phys., 70, 1679–1693, doi:10.1016/j.jastp. 2008.06.008.

Shprits Y.Y., Subbotin D.A., Meredith N.P., Elkington S. (2008b), Review of modeling of losses and sources of relativistic electrons in the outer radiation belt II: local acceleration and losses. J. Atmos. Solar-Terr. Phys. vol. 70, pp. 1694–1713. DOI: 10.1016/j.jastp.2008.06.014.

Shprits, Y., M. Daae, and B. Ni (2012), Statistical analysis of phase space density buildups and dropouts, J. Geophys. Res., 117,A01219, doi:10.1029/2011JA016939

Shprits, Y. Y., A. Kellerman, N. Aseev,A. Y. Drozdov, and I. Michaelis (2017), Multi-MeV electron loss in the heart of the radiation belts, Geophys. Res. Lett.,44, 1204--1209, doi:10.1002/2016GL072258

Sheeley, N. R., Walters, J. H., Wang, Y. M., and Howard, R. A. (1999). Continuous Tracking of Coronal Outflows: Two Kinds of Coronal Mass Ejections. J. Geophys. Res. 104, 24739–24768. doi:10.1029/1999JA900308

Schulz, M., and L. Lanzerotti (1974), Particle Diffusion in the Radiation Belts, Springer, New York.

Staples, F. A., Rae, I. J., Forsyth, C., Smith, A. R. A., Murphy, K. R., Raymer, K. M., et al. (2020). Do statistical models capture the dynamics of the magnetopause during sudden magnetospheric compressions? *Journal of Geophysical Research: Space Physics*, *125*, e2019JA027289. https://doi.org/10.1029/2019JA027289

Shue, J.-H., Chao, J., Fu, H., Russell, C., Song, P., Khurana, K., & Singer, H. (1997). A new functional form to study the solar wind control of the magnetopause size and shape. *Journal of Geophysical Research*, *102*(A5), 9497–9511. https://doi.org/10.1029/97JA00196

Srivastava, N., and P. Venkatakrishnan (2004), Solar and interplanetary sources of major geomagnetic storms during 1996–2002, J. Geophys. Res., 109, A10103, doi:10.1029/2003JA010175.

Turner, D. L., T. P. O'Brien, J. F. Fennell, S. G. Claudepierre, J. B. Blake, E. K. J. Kilpua, and H. Hietala (2015), The effects of geomagnetic storms on electrons in Earth's radiation belts, Geophys. Res. Lett., 42, doi:10.1002/2015GL064747

Tu, W., Selesnick, R., Li, X., & Looper, M. (2010). Quantification of the precipitation loss of radiation belt electrons observed by SAMPEX. *Journal of Geophysical Research*, *115*, A07210. https://doi.org/10.1029/2009JA014949.

Tu, W., G. S. Cunningham, Y. Chen, S. K. Morley, G. D. Reeves, J. B. Blake, D. N. Baker, and H. Spence (2014), Event-specific chorus wave and electron seed population models in DREAM3D using the Van Allen Probes, *Geophys. Res. Lett.*, 41, doi:10.1002/2013GL058819.

Tu, W., Xiang, Z., & Morley, S. K. (2019). Modeling the magnetopause shadowing loss during the June 2015 dropout event. *Geophysical Research Letters*, 46, 9388–9396. https://doi.org/10.1029/2019GL084419.

Turner, D. L., S. K. Morley, Y. Miyoshi, B. Ni, and C.-L. Huang (2012a). Outer Radiation Belt Flux Dropouts: Current Understanding and Unresolved Questions. Dynamics of the Earth's Radiation Belts and Inner Magnetosphere, edited by Danny Summers, et al., American Geophysical Union, 2013.

Turner et al. (2012b). Explaining sudden losses of outer radiation belt electrons during geomagnetic storms. Nature Physics, 8, 202–212. https://doi.org/10.1038/nphys2185

Turner, D. L., S. K. Morley, Y. Miyoshi, B. Ni, and C.-L. Huang (2013). Outer Radiation Belt Flux Dropouts: Current Understanding and Unresolved Questions in the Dynamics of the Earth's Radiation Belts and Inner Magnetosphere, edited by Danny Summers, et al., American Geophysical Union. ProQuest Ebook Central.

Thorne, R. M. (2010). Radiation belt dynamics: The importance of wave-particle interactions. Geophysical Research Letters, 37, L22107. https://doi.org/10.1029/2010GL044990

Tsyganenko, N. A., & Sitnov, M. I. (2005). Modeling the dynamics of the inner magnetosphere during strong geomagnetic storms. *Journal of Geophysical Research*, *110*, A03208. https://doi.org/10.1029/2004JA010798.

Thorne, R. M. et al. Rapid local acceleration of relativistic radiation-belt electrons by magnetospheric chorus. Nature 504, 411–414 (2013).

Wanliss, J. A., and K. M. Showalter (2006), High-resolution global storm index: Dst versus SYM-H, *J. Geophys. Res.*, *111*, A02202, doi:10.1029/2005JA011034

Wang, Y and Zhang, J. (2007), A comparative study between eruptive x-class flares associated with coronal mass ejections and confined x-class flares The Astrophysical Journal, 665:1428Y1438.

Webb, D. F., and Howard, T. A. (2012). Coronal Mass Ejections: Observations. Living Rev. Solar Phys. 9, 3. doi:10.12942/lrsp-2012-3

Wrenn, G. L. (1995). Conclusive evidence for internal dielectric charging anomalies on geosynchronous communications spacecraft. Journal of Spacecraft and Rockets,32, 514–520.

Whang, Y. C., D. Larson, R. P. Lin, R. P. Lepping, and A. Szabo (1998), Plasma and magnetic field structure of a slow shock: Wind observations in interplanetary space, Geophys. Res. Lett.,25, 2625.

Wrenn, G. L., Rodgers, D. J., & Ryden, K. A. (2002). A solar cycle of spacecraft anomalies due to internal charging. Annals of Geophysics,20,953–956.GLAUERT ET AL.1522

Xiang, Z., Tu, W., Ni, B., Henderson, M. G., & Cao, X. (2018). A statistical survey of radiation belt dropouts observed by Van Allen Probes. *Geophysical Research Letters*, *45*, 8035–8043. https://doi.org/ 10.1029/2018GL078907.

Xiang, Z., Tu, W., Li, X., Ni, B., Morley, S. K., & Baker, D. N. (2017). Understanding the mechanisms of radiation belt dropouts observed by Van Allen Probes. Journal of Geophysical Research: Space Physics, 122, 9858–9879. https://doi.org/10.1002/2017JA024487.

Yando, K., R. M. Millan, J. C. Green, and D. S. Evans (2011), A Monte Carlo simulation of the NOAA POES medium energy proton and electron detector instrument, J. Geophys. Res., 116, A10231, doi:10.1029/ 2011JA016671.

Yashiro, S., Gopalswamy, N., Michalek, G., Cyr, St. O. C., Plunkett, S. P., Rich, N. B., et al. (2004). A Catalog of White Light Coronal Mass Ejections Observed by the SOHO Spacecraft. J. Geophys. Res. (Space Phys.) 109, A07105. doi:10.1029/2003JA010282

Yuan, C., and Q. Zong (2013), Relativistic electron fluxes dropout in the outer radiation belt under different solar wind conditions, *J. Geophys. Res. Space Physics*, *118*, doi:10.1002/2013JA019066.

Zuo, P. B., F. S. Wei, and X. S. Feng (2006), Observations of an interplanetary slow shock associated with magnetic cloud boundary layer, Geophys. Res. Lett., 33, L15107, doi:10.1029/2006GL026419

Figure 1.

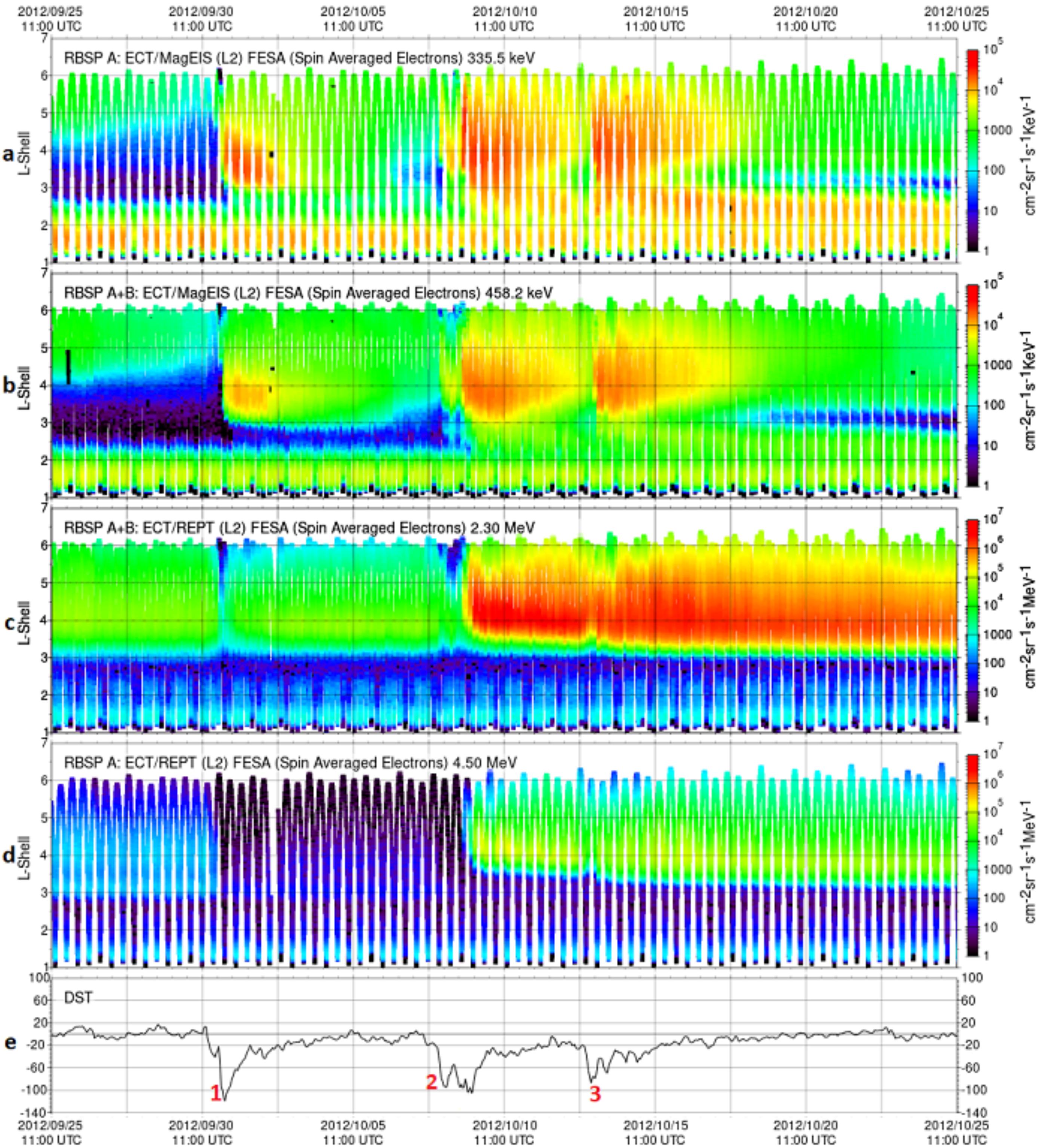

2012/09/25 11:00 UTC
2012/09/30 11:00 UTC
2012/10/05 11:00 UTC
2012/10/10 11:00 UTC
2012/10/15 11:00 UTC
2012/10/20 11:00 UTC
2012/10/25 11:00 UTC
a
RBSP A: ECT/MagEIS (L2) FESA (Spin Averaged Electrons) 335.5 keV
b
RBSP A+B: ECT/MagEIS (L2) FESA (Spin Averaged Electrons) 458.2 keV
c
RBSP A+B: ECT/REPT (L2) FESA (Spin Averaged Electrons) 2.30 MeV
d
RBSP A: ECT/REPT (L2) FESA (Spin Averaged Electrons) 4.50 MeV
L-Shell
$cm^{-2}sr^{-1}s^{-1}KeV^{-1}$
$cm^{-2}sr^{-1}s^{-1}MeV^{-1}$
e
DST
1
2
3

Figure 2.

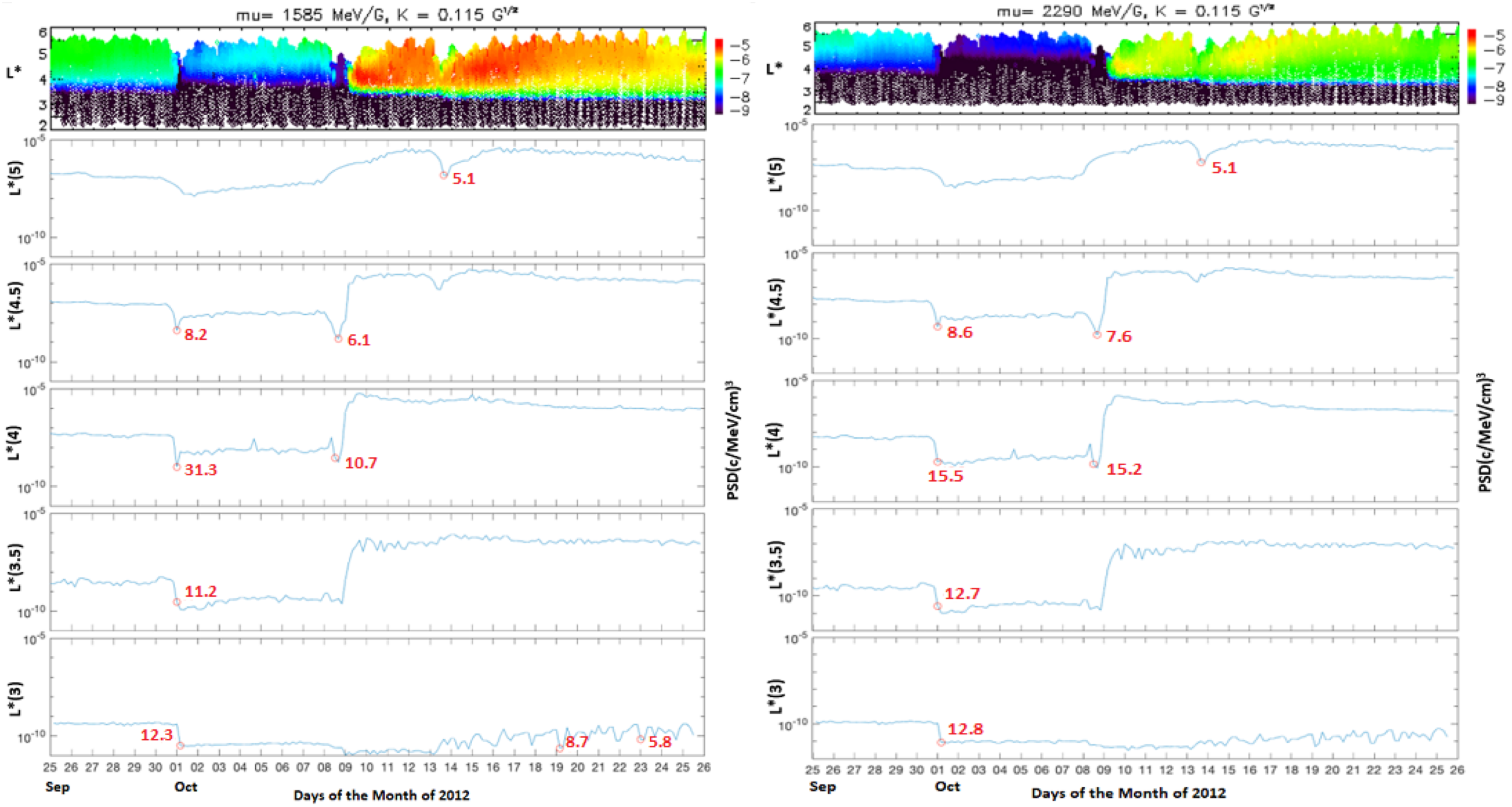

mu= 1585 MeV/G, K = 0.115 G^1/2
mu= 2290 MeV/G, K = 0.115 G^1/2
L*
L*(5)
L*(4.5)
L*(4)
L*(3.5)
L*(3)
PSD(c/MeV/cm)^3
5.1
8.2
6.1
31.3
10.7
11.2
12.3
8.7
5.8
8.6
7.6
15.5
15.2
12.7
12.8
Sep
Oct
Days of the Month of 2012

Figure 3.

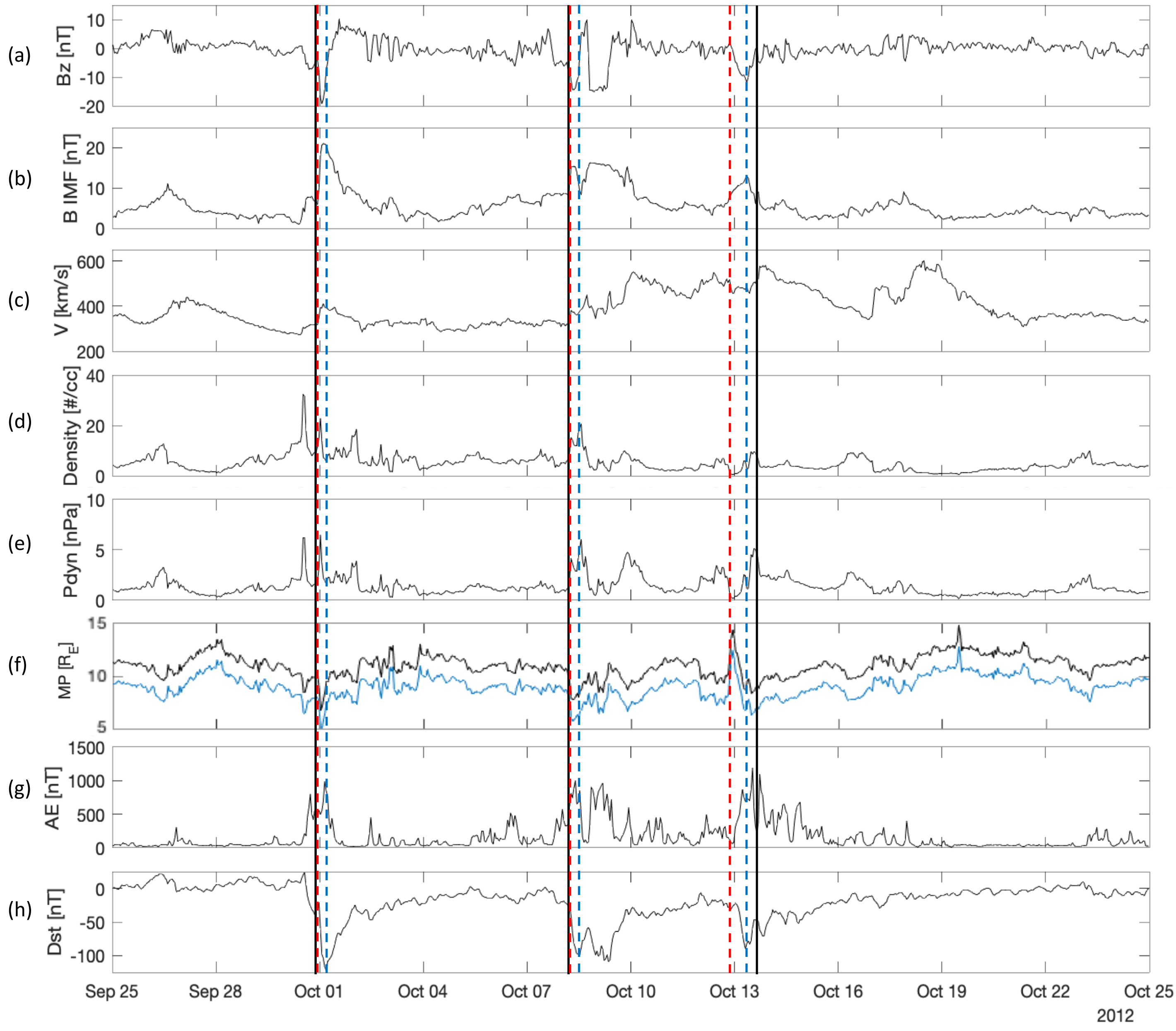
(a)
Bz [nT]
10
0
-10
-20
(b)
B IMF [nT]
20
10
0
(c)
V [km/s]
600
400
200
(d)
Density [#/cc]
40
20
0
(e)
Pdyn [nPa]
10
5
0
(f)
MP [R_E]
15
10
5
(g)
AE [nT]
1500
1000
500
0
(h)
Dst [nT]
0
-50
-100
Sep 25
Sep 28
Oct 01
Oct 04
Oct 07
Oct 10
Oct 13
Oct 16
Oct 19
Oct 22
Oct 25
2012

Figure 4.

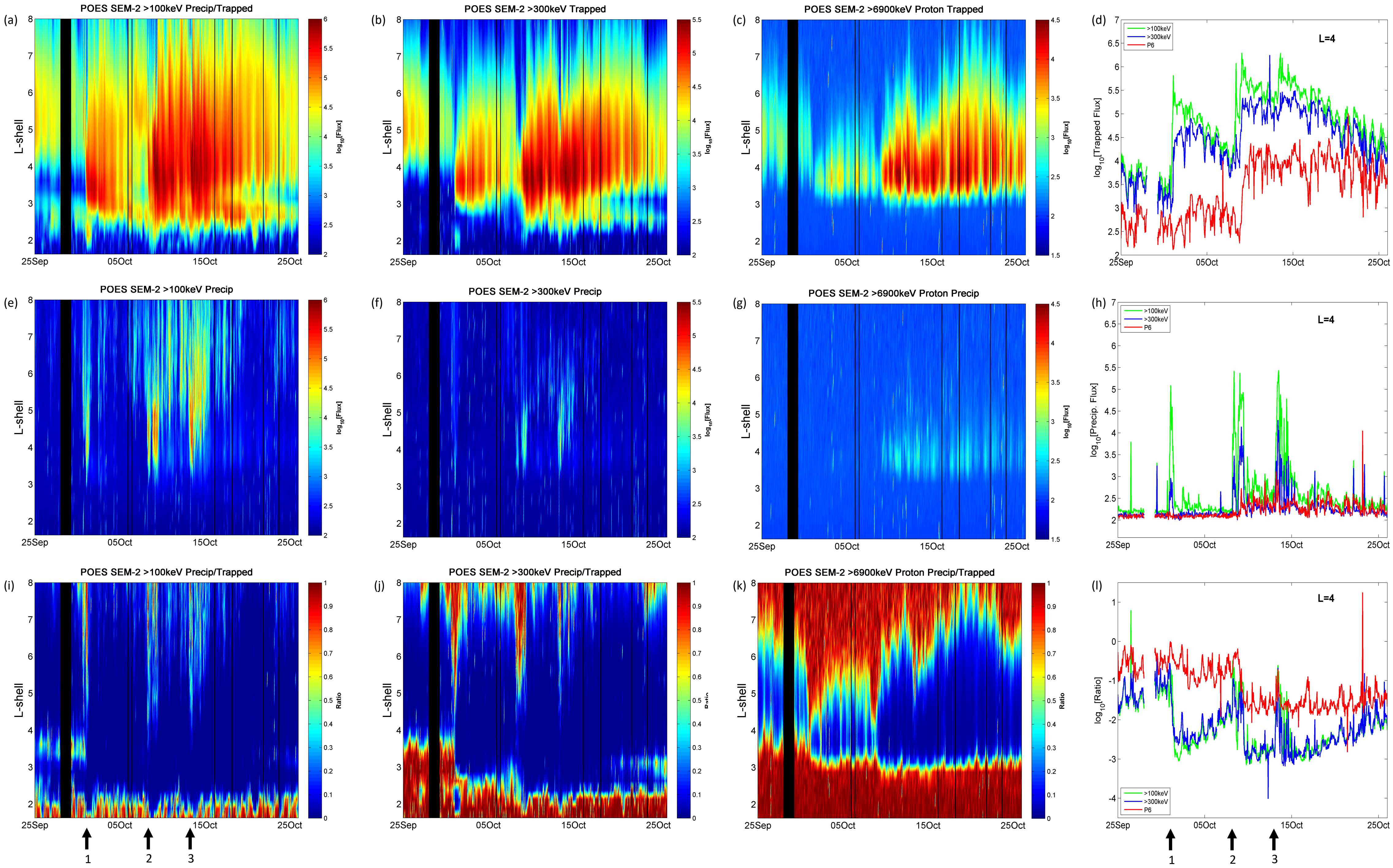
POES SEM-2 >100keV Precip/Trapped
POES SEM-2 >300keV Trapped
POES SEM-2 >6900keV Proton Trapped
POES SEM-2 >100keV Precip
POES SEM-2 >300keV Precip
POES SEM-2 >6900keV Proton Precip
POES SEM-2 >100keV Precip/Trapped
POES SEM-2 >300keV Precip/Trapped
POES SEM-2 >6900keV Proton Precip/Trapped
(a)
(b)
(c)
(d)
(e)
(f)
(g)
(h)
(i)
(j)
(k)
(l)
L-shell
log10[Flux]
Ratio
log10[Trapped Flux]
log10[Precip. Flux]
log10[Ratio]
L=4
>100keV
>300keV
P6
25Sep
05Oct
15Oct
25Oct
1
2
3